Published in final edited form as:
Traffic. 2012 March ; 13(3): 483–494. doi:10.1111/j.1600-0854.2011.01323.x.

Toxin Pores Endocytosed During Plasma Membrane Repair Traffic into the Lumen of MVBs for Degradation

Matthias Corrotte, **Maria Cecilia Fernandes**, **Christina Tam**, and **Norma W. Andrews***
Department of Cell Biology and Molecular Genetics, College of Computer, Mathematics and Natural Sciences, University of Maryland, College Park, MD, USA

Abstract

Cells permeabilized by the bacterial pore-forming toxin streptolysin O (SLO) reseal their plasma membrane in a Ca^{2+}-dependent manner. Resealing involves Ca^{2+}-dependent exocytosis of lysosomes, release of acid sphingomyelinase and rapid formation of endosomes that carry the transmembrane pores into the cell. The intracellular fate of the toxin-carrying endocytic vesicles, however, is still unknown. Here, we show that SLO pores removed from the plasma membrane by endocytosis are sorted into the lumen of lysosomes, where they are degraded. SLO-permeabilized cells contain elevated numbers of total endosomes, which increase gradually in size while transitioning from endosomes with flat clathrin coats to large multivesicular bodies (MVBs). Under conditions that allow endocytosis and plasma membrane repair, SLO is rapidly ubiquitinated and gradually degraded, in a process sensitive to inhibitors of lysosomal hydrolysis but not of proteasomes. The endosomes induced by SLO permeabilization become increasingly acidified and promote SLO degradation under normal conditions, but not in cells silenced for expression of Vps24, an ESCRT-III complex component required for the release of intraluminal vesicles into MVBs. Thus, cells dispose of SLO transmembrane pores by ubiquitination/ESCRT-dependent sorting into the lumen of late endosomes/lysosomes.

Keywords

endocytosis; ESCRT; lysosome; multivesicular body; repair; resealing; streptolysin O

Pore-forming toxins are an important class of bacterial virulence factors, which promote plasma membrane damage, pathogen escape from phagosomes or translocation of bacterial effectors into the cytosol (1). The cholesterol-dependent cytolysins (CDCs) contribute to the pathogenesis of a large number of Gram-positive bacteria by binding to the cell surface, oligomerizing and penetrating the membrane to form a large proteinaceous pore (2,3). Streptolysin O (SLO) is a CDC produced by *Streptococcus pyogenes* that has been extensively used as a permeabilization tool in cell biological studies (4,5). Interestingly, it recently became clear that although mammalian cells can remain permeabilized after exposure to high concentrations of SLO, a Ca^{2+}-dependent repair mechanism present in mammalian cells actively removes SLO pores from the plasma membrane, promoting full-

*Corresponding author: Norma W. Andrews, andrewsn@umd.edu.

Supporting Information

Additional Supporting Information may be found in the online version of this article

Please note: Wiley-Blackwell are not responsible for the content or functionality of any supporting materials supplied by the authors. Any queries (other than missing material) should be directed to the corresponding author for the article.

cell resealing at lower doses of the toxin (6,7). This repair mechanism is initiated by Ca^{2+} influx through the transmembrane pores, an event that triggers exocytosis of lysosomes (8,9) and extracellular release of the lysosomal enzyme acid sphingomyelinase. The hydrolytic activity of acid sphingomyelinase on the outer leaflet of the plasma membrane triggers a rapid form of endocytosis, which internalizes the pores and promotes plasma membrane repair (7,10). These findings led to a model proposing that cleavage of sphingomyelin head groups by secreted acid sphingomyelinase generates ceramide-enriched microdomains on the plasma membrane, leading to the formation of endocytic vesicles that carry the SLO pores into the cell (10).

The role of endocytosis in the repair of wounds caused by pore-forming proteins was subsequently confirmed in distinct systems, including *Caenorhabditis elegans*, and mammalian targets of the cytotoxic lymphocyte protein perforin (11,12). However, despite these advances, the intracellular fate of large transmembrane proteinaceous pores after internalization is still unknown. In this study, we investigate in detail the fate of SLO pores inserted into the membrane of NRK cells, and show that the toxin is ubiquitinated, travels through the endocytic pathway and is ultimately degraded after being sorted into the lumen of late endosomes/lysosomes.

Results and Discussion

Cell permeabilization by SLO pores induces formation of vesicles that traffic through the endocytic pathway

Earlier studies detected a rapid form of endocytosis in cells wounded in the presence of Ca^{2+}, and showed that this process is required for the internalization of plasma membrane lesions and cell resealing (7,10). To investigate the intracellular fate of these injury-induced endocytic vesicles, we examined cells permeabilized or not by the pore-forming toxin SLO in the presence of BSA-gold as an endocytic tracer. Figure 1 shows transmission electron microscopy (TEM) images of newly formed endocytic vesicles observed at various time-points. At 1 min, SLO-treated cells contained numerous large and irregular endosomes, when compared to control cells. After 5 min in SLO-treated cells, the tracer was present within larger endosomes showing flat electron-dense coats and low amounts of intraluminal vesicles. At this point, these endocytic vesicles were larger in size but similar in morphology to endosomes observed in control cells. These endosomes strongly resembled the endosomal vesicles shown in numerous studies to contain flat clathrin coats, and proposed to be involved in protein sorting toward lysosomes (13–15). At 15 min, BSA-gold-positive endosomes in SLO-treated cells were on average larger, and contained more internal vesicles than endosomes present in control cells not exposed to SLO. After 30 min, large BSA-gold-containing endosomes were observed in both SLO-treated as well as control cells, with a morphology typical of multivesicular bodies (MVBs) (16).

These results suggested that SLO-induced endosomes, although more numerous and larger than the endocytic vesicles normally observed in control cells, might also be following the classical progression from early endosomes to MVBs. Quantification of the average number of BSA-gold-positive vesicles over time revealed that SLO permeabilization significantly enhanced endosome formation (Figure 1B), consistent with previous reports (7). The average area of the endosomes formed in SLO-treated cells was also larger when compared to control cells (Figure 1C), consistent with an increased number of newly formed endosomes maturing and trafficking through the endocytic pathway.

To determine the maturation rate of the SLO-induced endosomes, we quantified the number of internal vesicles in TEM sections and classified them into early endosomes (based on the presence of less than five intraluminal vesicles and flat clathrin coats (15)) or late

endosomes/MVBs (based on the presence of more than six intraluminal vesicles (17)). As expected, the average number of internal vesicles per endosome profile increased over time in both SLO-treated and control cells, reflecting the traffic of internalized BSA-gold through the endocytic pathway. The average number of internal vesicles in BSA-gold-positive endosomes was significantly higher in SLO-treated cells than in control cells (Figure 2A). When endosomes displaying flat dense coats and less than six intraluminal vesicles (Figure 2D) were quantified as percentage of total vesicles, in SLO-treated cells there was also a progressive increase in the number of vesicles with early endosome features over time, followed by a sharp decrease between 15 and 30 min (Figure 2B). These results indicate that endocytic vesicles induced by SLO permeabilization enter and exit the early endosomal stage of maturation within a period of 30 min after their formation. This finding is consistent with a relatively faster transit rate of vesicles carrying SLO pores through the endocytic pathway. In control cells not exposed to the toxin, the numbers of early endosomes remained stable between 15 and 30 min, suggesting a slower maturation process. Quantification of the percentage of late endosomes/MVBs showed that after 15 min a higher fraction of the endocytosed BSA-gold was present in endosomes containing numerous intraluminal vesicles, and the occasional multilamellar structures that are typical of late stages of endosomal maturation (Figure 2C,E). One potential mechanism that may be responsible for the larger size and faster maturation rate of endosomes carrying SLO is Ca^{2+} release from the lumen of toxin-permeabilized endosomes, as luminal Ca^{2+} is known to play an important role in traffic through the late endocytic pathway (18).

SLO is endocytosed and travels along the endosomal pathway to MVBs/lysosomes

To follow the localization of SLO during cell permeabilization and resealing, a green fluorescent protein (GFP)-tagged SLO construct was generated and shown to have full pore-forming activity (Figure S1), comparable to untagged SLO (7). Cells were permeabilized with GFP-SLO in medium containing Ca^{2+} (conditions that allow pore removal by endocytosis and cell resealing (7)), and examined using cryo-EM immunostaining using anti-GFP antibodies. GFP-SLO was initially observed associated with the plasma membrane, and subsequently in intracellular vesicles, which increased in size over time (Figure 3A). Between 15 and 30 min after permeabilization, GFP-SLO was detected in association with large endosomes containing multiple intraluminal vesicles. At those later time-points, GFP-SLO was detected either at the limiting membrane or on the membrane of intraluminal vesicles (Figure 3A, 15 and 30 min). These observations suggest that plasma membrane-associated SLO enters late endosomes, and may be sorted into the lumen of MVBs/lysosomes.

The relative localization of GFP-SLO between the plasma membrane and the intracellular environment was quantified from the total GFP-SLO staining detected by cryo-EM immunostaining. When cells were fixed immediately after pre-incubation with GFP-SLO at 4°C for 5 min, >55% of the total cell-associated toxin was detected at the plasma membrane. When the temperature was elevated to 37°C in the presence of Ca^{2+} for various time-points after the initial permeabilization, the fraction of GFP-SLO located at the plasma membrane decreased to about 10% between 1 and 5 min, with a concomitant rapid increase in the fraction detected intracellularly (Figure 3B). These results indicate that after pore formation GFP-SLO rapidly leaves the plasma membrane and moves to an intracellular location, consistent with the detection of the toxin in endocytic vesicles (Figure 3A). The distance of intracellular GFP-SLO to the plasma membrane was quantified over time (Figure 3C), and the results show that SLO progressively moves away from the plasma membrane toward a perinuclear site, in a pattern that is typical of the progression along the endosomal pathway from early to late endosomes/MVBs (19).

A recent study proposed that SLO pores are removed from the plasma membrane through blebbing, and not by endocytosis (20). Indeed, cells permeabilized by SLO and other pore-forming proteins show intense blebbing, as documented in an earlier study from our laboratory (7). However, Keyel et al. (20) neglected to mention that Idone et al. (7) had addressed in detail the role of blebbing in SLO pore removal, and ruled it out based on the extensive experimental evidence. Time-lapse imaging revealed that blebs induced by SLO are not shed, but rapidly retract as the cells reseal (7). This observation is fully consistent with earlier findings, showing that bleb retraction is driven by reassembly of the actin contractile cortex (21). Importantly, disassembly of the cortical actin cytoskeleton with cytochalasin D eliminated blebbing after SLO permeabilization, but endocytosis and plasma membrane repair proceeded normally (7). In view of these findings, it is likely that the bleb shedding reported by Keyel et al. (20) resulted from the non-physiological conditions of the study, which in some experiments included fixation with formaldehyde and/or glutaraldehyde prior to exposure to SLO.

To confirm that the internalized GFP-SLO was trafficking to late endosomes/lysosomes, we performed double immunostaining of GFP and Lamp1 (a marker of late endosomes/lysosomes) in cells pretreated with GFP-SLO and further incubated for 30 min (Figure 3D). At that time-point extensive colocalization of GFP-SLO (10 nm gold) with Lamp1 (5 nm gold) was observed on large multivesicular endosomes. These findings support the view that SLO traffics to late endosomes/lysosomes after being removed from the plasma membrane by endocytosis.

Endosomes carrying SLO mature into acidic compartments where the toxin is degraded

Having determined that internalized SLO traffics into late endosomal/lysosomal structures, we next assessed the intracellular fate of the toxin. After pretreatment with GFP-SLO, cells were incubated at 37°C for increasing periods of time under conditions that promote endocytosis and cell resealing (Ca^{2+}-containing medium) or conditions that do not allow pore internalization (Ca^{2+}-free medium), followed by cell lysis, pulldown of total GFP-SLO with GFP-Trap® agarose beads and western blot. In the presence of Ca^{2+}, the amount of cell-associated GFP-SLO was progressively reduced. In contrast, in Ca^{2+}-free conditions, there was significantly less loss in GFP-SLO over time (Figure 4A,B). This suggests that under conditions that promote plasma membrane repair after SLO pore formation the toxin is gradually degraded intracellularly, in agreement with the observed trafficking of SLO from toxin-induced early endosomes to MVB/lysosomal compartments (Figure 3D). The kinetics of SLO degradation is consistent with the cryo-EM immunostaining data in Figure 3, which shows the arrival of SLO in large perinuclear endocytic compartments containing luminal vesicles by 15–30 min.

In agreement with the view that internalized SLO is degraded in late endosomes/lysosomes, we found that the endosomes induced by cell permeabilization with SLO became increasingly acidified over time, acquiring the conditions necessary for protein degradation. Cells permeabilized with SLO were allowed to endocytose DQ Red-BSA, a self-quenched BODIPY dye conjugated to BSA that requires hydrolytic cleavage in an acidic compartment to generate a highly fluorescent product (22). Confocal microscopy revealed a progressive increase in the level of DQ-BSA fluorescence within intracellular vesicles after increasing periods following SLO permeabilization (Figure 4C,D), consistent with the larger number of endosomes formed in these cells becoming acidified and hydrolytic over time. As dequenching of DQ-BSA requires residence in acidified compartments, the overall kinetics of fluorescence increase was delayed, relative to the kinetics of SLO degradation (Figure 4A). Nonetheless, a significant increase in DQ-BSA fluorescence was detectable in SLO-treated cells as early as 30 min after treatment, which is consistent with degradation kinetics of GFP-SLO. Treatment with bafilomycin A (BafA), a v-ATPase inhibitor that blocks

endosomal acidification, led to a strong reduction in DQ-BSA fluorescence confirming that cleavage of this dye requires arrival in acidic compartments (Figure 4C,D). In agreement with the conclusion that the amount of DQ-BSA cleavage reflects the extent of endocytosis after SLO pore formation, we found that the intracellular accumulation of dequenched DQ-BSA increases proportionally to the dose of SLO added to cells. After pretreatment with SLO and DQ-BSA followed by a chase of 2 h (to allow full dequenching of DQ-BSA after arrival in late endosomes/lysosomes), the total cell-associated fluorescence intensity increased steadily from 70 to 250 ng/mL SLO (Figure 4E).

To confirm that SLO is degraded in late endosomes/lysosomes, we performed GFP-SLO pull-down assays after 5 and 30 min in cells pretreated or not with lysosomal inhibitors (concanamycin A and leupeptin) or a proteasome inhibitor (MG132). In untreated cells, the amount of cell-associated GFP-SLO was markedly reduced at 30 min (Figure 4F), consistent with the period required for the toxin to enter late endosomal/lysosomal compartments (Figure 3A–D), where degradation occurs. However, in cells treated with lysosomal inhibitors SLO levels remained high after 30 min, whereas treatment with a proteasome inhibitor allowed degradation (Figure 4F). Taken together, these results strongly suggest that SLO entering cells during plasma membrane repair traffics into the lumen of acidic late endosomes, where it is degraded by lysosomal enzymes. Interestingly, heptamer complexes of the pore-forming protein alpha-toxin were also reported to be internalized by mammalian cells and traffic to late endosomes, but their loss from cells was not blocked by lysosomal inhibitors (23). The degradative route followed by SLO pores may be linked to their ability to form large pores and trigger Ca^{2+} influx and Ca^{2+}-dependent repair, as resealing after permeabilization with the significantly smaller alpha-toxin pores was described to be Ca^{2+} independent (23). These observations are consistent with the distinct signaling pathways triggered after attack by alpha-toxin or SLO (24,25).

After endocytosis, SLO assembled into transmembrane pores is ubiquitinated and sorted by the ESCRT complex into the lumen of lysosomes for degradation

The initial permeabilization of cells exposed to SLO in the presence of Ca^{2+}, followed by removal of the toxin by endocytosis (7), indicates that SLO enters cells in the form of transmembrane pores which initially reside in the plasma membrane and are subsequently incorporated into the limiting membrane of endosomes (Figure 3A–D). Thus, to allow degradation in the acidified lysosomal lumen (Figure 4A–F), it would be necessary for SLO to be recognized by a cellular machinery capable of sorting the toxin pore into the lumen, while preserving the integrity of the compartment. To examine this issue, we determined if SLO was modified by ubiquitin, the classical signal that determines processing of membrane proteins along the endocytic pathway (26,27). To this end, we used the ubiquitin association domain (UBA) (28,29) coupled to agarose to pulldown the total fraction of ubiquitinated proteins in cell lysates, and analyzed this fraction for the presence of SLO. Immunoblots detected GFP-SLO in the fraction of ubiquitinated proteins 1 min after cell permeabilization and plasma membrane repair. The amounts of SLO present in this fraction decreased rapidly, indicating that the ubiquitination step occurs at early stages after cell permeabilization. In the absence of Ca^{2+}, a condition that does not promote SLO endocytosis and plasma membrane resealing, only trace amounts of SLO were detected in the total fraction of ubiquitinated proteins (Figure 5A, upper panel). This suggests that the Ca^{2+}-dependent plasma membrane repair process, which involves rapid formation of endocytic vesicles and toxin internalization (7,10), is necessary for the early ubiquitination of SLO. The specificity of this assay in detecting ubiquitinated SLO was confirmed by parallel pulldowns using a mutated UBA domain (Figure 5A, lower panel). In addition, pulldown of GFP-SLO using GFP-Trap agarose followed by immunoblot with anti-ubiquitin antibodies showed the same pattern observed with UBA pulldowns: ubiquitinated GFP-SLO

was present 1 min after SLO permeabilization in the presence of Ca^{2+}, while significantly reduced amounts were observed in the absence of Ca^{2+} (Figure 5B). This result confirms that SLO is directly ubiquitinated, shortly after internalization.

At the level of early endosomes, ubiquitinated membrane proteins can be recognized and processed by the ESCRT complex, which is involved in sorting ubiquitinated proteins into the intraluminal vesicles of MVBs for degradation (30). The ESCRT complex acts through the sequential recruitment and action of several proteins designated as ESCRT-0, -I, -II and -III, which are essential for the proper sorting of membrane proteins into the vesicles that invaginate into the luminal space of MVBs (31,32). To determine the involvement of this pathway in the sorting and degradation of SLO, we used small interfering RNA (siRNA) duplexes to silence expression of VPS24, a member of the ESCRT-III complex that is required for the final step of releasing intraluminal vesicles containing membrane proteins into the MVB lumen (33,34). Strong knockdown of Vps24 was achieved in comparison with control siRNA (Figure 5C). These Vps24-depleted cells were still able to reseal their plasma membrane after SLO permeabilization in the presence of Ca^{2+}, as determined in propidium iodide (PI) exclusion assays (results not shown). After pretreatment with GFP-SLO, pull-down assays were performed to assess the level of degradation of SLO after 5, 15 and 30 min. The progressive degradation of GFP-SLO that is observed in control cells was strongly inhibited after treatment with Vps24 siRNA (Figure 5C,D). Thus, Vps24 is required for the lysosomal degradation of SLO trafficking through the endocytic pathway, similar to what has been reported for endogenous membrane proteins (33). These results suggest that ubiquitin added to SLO promotes its recognition by the ESCRT machinery, resulting in sorting of the toxin into the lumen of MVBs for degradation. This conclusion is reinforced by our frequent observation of flat dense lattices resembling clathrin coats in SLO-induced endosomes (Figures 1 and 2), which are thought to represent sites where ubiquitinated membrane proteins are recognized by ESCRT-0 components (14). The Vps24 requirement for SLO degradation reinforces the view that the toxin is trafficking intracellularly as a transmembrane pore, as Vps24 is not essential for fluid-phase transport between early endosomes and lysosomes (33).

If SLO traffics into late endosomes/lysosomes as a multimer assembled as a transmembrane pore, one prediction is that endosomes carrying the toxin would only be able to reach the low pH required for degradation after the pores are sorted into MVB intraluminal vesicles. To investigate this question, we performed DQ-BSA uptake assays in control and Vps24-depleted cells, treated or not with SLO (Figure 5E,F). In cells not exposed to SLO, which undergo constitutive endocytosis, no significant difference was observed between control and Vps24-depleted cells. This result indicates that the endocytosis of DQ-BSA and the acidification necessary for DQ-BSA dequenching is not impaired in the absence of Vps24 [Figure 5E (left panels),F], consistent with previous findings (33). Following SLO treatment, the DQ-BSA fluorescence intensity was markedly increased in cells treated with control siRNA, as previously shown in Figure 4C. However, in Vps24-depleted cells, SLO treatment did not increase DQ-BSA fluorescence, which remained at levels seen in cells not exposed to SLO [Figure 5E (right panels),F]. These results suggest that in the absence of Vps24, SLO pores remain at the limiting membrane of endosomes, impairing compartment acidification and hydrolase activity. The conclusion that SLO pores on the limiting membrane of endosomes account for the inhibition in acidification is supported by a prior report that FITC-EGF-containing endosomes in Vps24-depleted cells show the same low pH as control cells (33). However, as knockdown of Vps24 leads to smaller endosomes lacking intraluminal vesicles of a homogeneous size (32,33), the reduction in dequenched DQ-BSA accumulation may also be related to changes in endosomal morphology. It is noteworthy that changes in lipid composition have also been linked to the formation of intraluminal vesicles in MVBs (35), but there is evidence that an acidic luminal pH may be required for

this process (36,37). As the presence of a pore in the limiting membrane of endosomes is predicted to impair acidification, it is conceivable that the SLO sorting process we observed relies primarily on the ESCRT complex machinery, which may still be capable of promoting luminal vesicle formation in the absence of full acidification.

Previous work showed that the endocytic process that follows cell permeabilization with SLO is a result of Ca^{2+}-triggered exocytosis of the lysosomal enzyme acid sphingomyelinase (10). Thus, in principle, not all endosomes induced by SLO permeabilization would have to carry SLO pores, as ceramide-enriched domains generated on the outer leaflet of the plasma membrane by acid sphingomyelinase might be formed in the vicinity of permeabilization sites, and generate endocytic vesicles through inward budding (10). However, our observations in Vps24-depleted cells appear to indicate that under our experimental conditions pores were present on most SLO-induced endosomes, as silencing of the component required for sorting of the pore into the lumen of MVBs reduced the level of DQ-BSA fluorescence to levels comparable to those observed without the toxin.

Taken together, our results reveal the mechanism by which cells ultimately dispose of transmembrane toxin pores inserted into their plasma membrane. This cellular recovery process can be separated into two phases: (i) the rapid formation of endocytic vesicles that remove toxin pores from the plasma membrane (7,10) and (ii) the ubiquitination of SLO and maturation of the toxin-induced endosomes, which leads to partition of the transmembrane pores into the lumen of MVBs and degradation (see model in Figure 6). Our findings extend previous reports showing that exogenous pathogen proteins can be recognized by the cellular ubiquitination machinery (38,39) and demonstrate that ubiquitinated transmembrane bacterial toxins functionally interact with components of the ESCRT pathway.

Materials and Methods

Cells and antibodies

NRK cells were cultured at 37°C in 5% CO_2 in high glucose DMEM containing 10% heat-inactivated FBS and penicillin/streptomycin (Invitrogen). Immunoblot and immuno-EM assays were performed using rabbit anti-GFP to detect GFP-SLO (Invitrogen), rabbit anti-ubiquitin (Abcam), rabbit anti Vps24 (Santa Cruz Biotechnology), mouse anti-actin (Sigma) and mouse anti-Lamp1 monoclonal antibodies (mAb) (LYIC6; provided by I. Mellman, Genentech).

Drug treatments

Cells were treated in DMEM containing 10% FBS with 250 nM concanamycin A (Sigma) and 100 μM leupeptin (Sigma) or 10 μM MG132 (American Peptide Company) for 2 h at 37°C followed by GFP-SLO permeabilization and toxin intracellular degradation assays.

Transcriptional silencing of Vps24

NRK cells (50% confluency) in 75-cm^2 flasks containing reduced serum DMEM without penicillin/streptomycin were transfected with Lipofectamine siRNA Max (Invitrogen) and 960 pmol of medium content control or Vps24 stealth siRNA duplexes, according to the manufacturer's instructions (Invitrogen). After 48 h of transfection, cells were permeabilized with GFP-SLO and analyzed for intracellular degradation or DQ-BSA uptake.

Cell permeabilization and repair assay

SLO and GFP-SLO were purified from BL21 *Escherichia coli* expressing 6× histidine-tagged toxin, as previously described (7). GFP-SLO was constructed by inserting GFP N-terminal to SLO into pTrcHisA-SLO (plasmid containing SLO carrying a cysteine deletion

that eliminates the need for thiol activation, provided by R. Tweeten, University of Oklahoma), using the same engineered *SalI* sites previously described for the generation of Cherry-SLO (7). Prior to exposure to the toxin, cell monolayers (60% confluence) were washed at 4°C with Ca^{2+}-free DMEM (containing Mg^{2+} and 10 mM EGTA), followed by two more washes in Ca^{2+}-free DMEM. GFP-SLO was bound to target cells in Ca^{2+}-free DMEM for 5 min at 4°C, and pore formation followed by plasma membrane repair was triggered by replacing the medium with 37°C DMEM containing or not 1.8 mM Ca^{2+}, for various periods of time. In all experiments, cells were treated with concentrations of GFP-SLO that allowed extensive permeabilization without inducing cell loss (concentrations ranged from 70 to 250 ng/mL).

PI membrane repair assay

Cells were cultured on coverslips at 60% confluence, treated for 5 min at 4°C with increasing concentrations of GFP-SLO and shifted to 37°C with or without Ca^{2+} for 4 min before adding 50 μg/mL PI (Sigma) for 1 min to assess pore formation and membrane repair. Cells were then fixed with 4% Paraformaldehyde (PFA), DAPI stained and imaged with a Zeiss Axiovert 200 using a 10× objective. Quantifications were performed by counting all DAPI- and PI-stained nuclei in five random fields (>300 cells) and determining the percentage of PI-positive nuclei in each field.

GFP-SLO pull-down assay

Cells were cultured to 60% confluence in 75-cm^2 flasks, treated for 5 min at 4°C with GFP-SLO and cell permeabilization and repair induced at 37°C with or without Ca^{2+} for various time-points. Cells were washed in Ca^{2+}-free cold PBS and solubilized in 1 mL of lysis buffer containing Tris–HCl (20 mM), NaCl (300 mM), $MgCl_2$ (1 mM), DTT (0.1 mM), EDTA (5 mM), Triton-X-100 (1%) and protease inhibitor cocktail (Roche) for 30 min at 4°C. After centrifugation to eliminate nuclei, supernatants were separated in two fractions, one saved as whole cell fraction (100 μL) and another (900 μL) that was incubated with 20 μL of GFP-Trap® agarose beads (Chromotek). After periods ranging from 4 h to overnight at 4°C, the samples were centrifuged at 2000× ***g*** for 2 min at 4°C, the pellets washed twice with washing buffer (lysis buffer without Triton-X-100) and resuspended in SDS sample buffer and boiled at 95°C for 10 min before performing SDS–PAGE and western blot assays with mouse anti-GFP mAbs.

UBA pull-down assay

Lysates of GFP-SLO-treated cells, prepared as described above for GFP-SLO pull-down assays, were incubated with the UBA (Dsk2p-UBA-GST) domain (28) or a mutant version, UBAmut (Dsk2p-UBAmut-GST) coupled to agarose beads (40 μL per sample, overnight at 4°C), to pull-down ubiquitinated proteins. Preparation of UBA domain/agarose beads was performed as described (29). Samples were then washed twice with cold washing buffer, resuspended in SDS sample buffer and boiled at 95°C for 10 min before performing SDS–PAGE and western blot assays using rabbit anti-GFP antibodies (Invitrogen) to detect GFP-SLO.

Western blot and densitometry

Following extraction and/or pulldown, proteins were separated on 8 or 10% polyacrylamide gels by SDS–PAGE and blotted on nitrocellulose membranes using the Trans-Blot Transfer system (Bio-Rad Laboratories) overnight at 30 V. After incubation with the primary antibodies and peroxidase-conjugated secondary antibodies, detection was performed using Supersignal West Pico Chemiluminescent Substrate (Thermo Scientific) and the Fuji

LAS-3000 Imaging System and Image Reader LAS-3000 software. Western blot densitometry analysis was performed using ImageJ gel analysis tools.

DQ-BSA uptake assay and quantification of acidic compartments

Following exposure to GFP-SLO, cells were incubated for 10 min with 1 mg/mL DQ Red-BSA (DQ-BSA, Invitrogen) in FBS-free DMEM at 37°C. After extensive washes with PBS, samples were chased at 37°C in FBS-free DMEM containing or not 100 nM BafA (Sigma) for 30 min, 1 or 2 h. After fixation with 4% PFA and DAPI staining, coverslips were imaged with a Leica SPX5 confocal system with 63× N.A. 1.4 oil objective. Z stacks (0.13 μm Z step between optical sections) of a minimum of five random fields (at least 250 cells) for each time-point were imaged. Stacks of individual channels were then imported to Volocity Suite (PerkinElmer), the total fluorescence intensity of the channel per microscopic field was determined (intensity × voxel count) and the values were normalized by the number of cells in each field (determined by DAPI staining).

Transmission EM

Cells treated with GFP-SLO for 5 min at 4°C and further incubated for various time-points at 37°C in Ca^{2+}/DMEM containing BSA-gold (OD of 520 nm = 200; (40)) were processed for TEM as previously described (8). Quantifications were performed by counting all vesicles containing BSA-gold in 16–57 cell sections/sample (which contained a total of 123–242 vesicles). Vesicle area was measured using the outline function of ImageJ, and the number of gold particles and internal vesicles was quantified for each BSA-gold-positive vesicle, in all vesicles found in the sections analyzed.

Cryo-EM immunolabeling

Cells were treated as described above for TEM and fixed in 4% PFA, 0.25 M HEPES and 0.1% glutaraldehyde for 1 h. Samples were rinsed, resuspended in 10% gelatin, chilled and trimmed to smaller blocks, placed in 2.3 M sucrose cryoprotectant overnight and frozen in liquid nitrogen. The frozen blocks were trimmed on a Leica Cryo-EMUC6 UltraCut and 65–70 nm sections were collected using the Tokuyasu method (41). The sections were collected on a drop of sucrose, placed on a nickel formvar/carbon-coated grid and floated in a dish of PBS prior to immunolabeling. For immunolabeling, grids were incubated with 0.1 M ammonium chloride to quench untreated aldehyde groups and blocked on 1% fish skin gelatin in PBS. Single-labeled grids were incubated with a primary rabbit anti-GFP antibody (Invitrogen; 1:50) followed by 10-nm protein A gold (Utrecht-UMC). Double-labeled grids were treated with an additional primary mouse anti-Lamp1 (LYIC6; provided by I. Mellman, Genentech; 1:20), bridged with rabbit anti-mouse (JacksonImmuno; 1:200) and incubated with 5-nm protein A gold. Grids were rinsed in PBS, fixed using 1% glutaraldehyde, rinsed, transferred to a UA/methylcellulose, dried and viewed in an FEI Tencai Biotwin electron microscope at 80 kV. Images were acquired using Morada charge-coupled device and item (Olympus) software. Quantification was performed by counting all GFP-SLO gold particles in 10–17 cell sections, which contained 175–500 gold particles. Distances between gold particles and the plasma membrane were measured using the line tool of ImageJ.

Supplementary Material

Refer to Web version on PubMed Central for supplementary material.

Acknowledgments

We thank Morven Graham and Kimberly Zichichi (EM facility, Center for Cell and Molecular Imaging, Yale University School of Medicine) for EM, Dr Andrew Flannery (University of Maryland) and Dr Nia Bryant (University of Glasgow) for UBA constructs, and members of the Andrews laboratory for helpful discussions.

References

1. Iacovache I, van der Goot FG, Pernot L. Pore formation: an ancient yet complex form of attack. Biochim Biophys Acta. 2008; 1778:1611–1623. [PubMed: 18298943]
2. Tweten RK. Cholesterol-dependent cytolysins, a family of versatile pore-forming toxins. Infect Immun. 2005; 73:6199–6209. [PubMed: 16177291]
3. Heuck AP, Moe PC, Johnson BB. The cholesterol-dependent cytolysin family of Gram-positive bacterial toxins. Subcell Biochem. 2010; 51:551–577. [PubMed: 20213558]
4. Koffer A, Gomperts BD. Soluble proteins as modulators of the exocytotic reaction of permeabilised rat mast cells. J Cell Sci. 1989; 94:585–591. [PubMed: 2698892]
5. Tan A, Bolscher J, Feltkamp C, Ploegh H. Retrograde transport from the Golgi region to the endoplasmic reticulum is sensitive to GTP gamma S. J Cell Biol. 1992; 116:1357–1367. [PubMed: 1541633]
6. Walev I, Bhakdi SC, Hofmann F, Djonder N, Valeva A, Aktories K, Bhakdi S. Delivery of proteins into living cells by reversible membrane permeabilization with streptolysin-O. Proc Natl Acad Sci U S A. 2001; 98:3185–3190. [PubMed: 11248053]
7. Idone V, Tam C, Goss JW, Toomre D, Pypaert M, Andrews NW. Repair of injured plasma membrane by rapid Ca2+-dependent endocytosis. J Cell Biol. 2008; 180:905–914. [PubMed: 18316410]
8. Rodriguez A, Webster P, Ortego J, Andrews NW. Lysosomes behave as Ca2+-regulated exocytic vesicles in fibroblasts and epithelial cells. J Cell Biol. 1997; 137:93–104. [PubMed: 9105039]
9. Reddy A, Caler E, Andrews N. Plasma membrane repair is mediated by Ca2+-regulated exocytosis of lysosomes. Cell. 2001; 106:157–169. [PubMed: 11511344]
10. Tam C, Idone V, Devlin C, Fernandes MC, Flannery A, He X, Schuchman E, Tabas I, Andrews NW. Exocytosis of acid sphingomyelinase by wounded cells promotes endocytosis and plasma membrane repair. J Cell Biol. 2010; 189:1027–1038. [PubMed: 20530211]
11. Los FC, Kao CY, Smitham J, McDonald KL, Ha C, Peixoto CA, Aroian RV. RAB-5- and RAB-11-dependent vesicle-trafficking pathways are required for plasma membrane repair after attack by bacterial pore-forming toxin. Cell Host Microbe. 2011; 9:147–157. [PubMed: 21320697]
12. Thiery J, Keefe D, Saffarian S, Martinvalet D, Walch M, Boucrot E, Kirchhausen T, Lieberman J. Perforin activates clathrin- and dynamin-dependent endocytosis, which is required for plasma membrane repair and delivery of granzyme B for granzyme-mediated apoptosis. Blood. 2010; 115:1582–1593. [PubMed: 20038786]
13. Ramm G, Pond L, Watts C, Stoorvogel W. Clathrin-coated lattices and buds on MHC class II compartments do not selectively recruit mature MHC-II. J Cell Sci. 2000; 113:303–313. [PubMed: 10633081]
14. Raiborg C, Wesche J, Malerod L, Stenmark H. Flat clathrin coats on endosomes mediate degradative protein sorting by scaffolding Hrs in dynamic microdomains. J Cell Sci. 2006; 119:2414–2424. [PubMed: 16720641]
15. Sachse M, Urbé S, Oorschot V, Strous GJ, Klumperman J. Bilayered clathrin coats on endosomal vacuoles are involved in protein sorting toward lysosomes. Mol Biol Cell. 2002; 13:1313–1328. [PubMed: 11950941]
16. Russell MRG, Nickerson DP, Odorizzi G. Molecular mechanisms of late endosome morphology, identity and sorting. Curr Opin Cell Biol. 2006; 18:422–428. [PubMed: 16781134]
17. Piper RC, Katzmann DJ. Biogenesis and function of multivesicular bodies. Annu Rev Cell Dev Biol. 2007; 23:519–547. [PubMed: 17506697]
18. Luzio JP, Bright NA, Pryor PR. The role of calcium and other ions in sorting and delivery in the late endocytic pathway. Biochem Soc Trans. 2007; 35:1088–1091. [PubMed: 17956286]

19. Gruenberg J, Maxfield FR. Membrane transport in the endocytic pathway. Curr Opin Cell Biol. 1995; 7:552–563. [PubMed: 7495576]
20. Keyel PA, Loultcheva L, Roth R, Salter RD, Watkins SC, Yokoyama WM, Heuser JE. Streptolysin O clearance through sequestration into blebs that bud passively from the plasma membrane. J Cell Sci. 2011; 124:2414–2423. [PubMed: 21693578]
21. Charras GT, Hu CK, Coughlin M, Mitchison TJ. Reassembly of contractile actin cortex in cell blebs. J Cell Biol. 2006; 175:477–490. [PubMed: 17088428]
22. Fader CM, Sanchez D, Furlan M, Colombo MI. Induction of autophagy promotes fusion of multivesicular bodies with autophagic vacuoles in k562 cells. Traffic. 2008; 9:230–250. [PubMed: 17999726]
23. Husmann M, Beckmann E, Boller K, Kloft N, Tenzer S, Bobkiewicz W, Neukirch C, Bayley H, Bhakdi S. Elimination of a bacterial pore-forming toxin by sequential endocytosis and exocytosis. FEBS Lett. 2009; 583:337–344. [PubMed: 19101547]
24. Husmann M, Dersch K, Bobkiewicz W, Beckmann E, Veerachato G, Bhakdi S. Differential role of p38 mitogen activated protein kinase for cellular recovery from attack by pore-forming *S. aureus* alpha-toxin or streptolysin O. Biochem Biophys Res Commun. 2006; 344:1128–1134. [PubMed: 16643845]
25. Aroian R, van der Goot FG. Pore-forming toxins and cellular non-immune defenses (CNIDs). Curr Opin Microbiol. 2007; 10:57–61. [PubMed: 17234446]
26. Hicke L, Dunn R. Regulation of membrane protein transport by ubiquitin and ubiquitin-binding proteins. Annu Rev Cell Dev Biol. 2003; 19:141–172. [PubMed: 14570567]
27. Hurley JH, Stenmark H. Molecular mechanisms of ubiquitin-dependent membrane traffic. Annu Rev Biophys. 2011; 40:119–142. [PubMed: 21332354]
28. Funakoshi M, Sasaki T, Nishimoto T, Kobayashi H. Budding yeast Dsk2p is a polyubiquitin-binding protein that can interact with the proteasome. Proc Natl Acad Sci U S A. 2002; 99:745–750. [PubMed: 11805328]
29. Lamb CA, McCann RK, Stockli J, James DE, Bryant NJ. Insulin-regulated trafficking of GLUT4 requires ubiquitination. Traffic. 2010; 11:1445–1454. [PubMed: 20854370]
30. Raiborg C, Stenmark H. The ESCRT machinery in endosomal sorting of ubiquitylated membrane proteins. Nature. 2009; 458:445–452. [PubMed: 19325624]
31. Hurley JH, Hanson PI. Membrane budding and scission by the ESCRT machinery: it's all in the neck. Nat Rev Mol Cell Biol. 2010; 11:556–566. [PubMed: 20588296]
32. Babst M. MVB vesicle formation: ESCRT-dependent, ESCRT-independent and everything in between. Curr Opin Cell Biol. 2011; 23:452–457. [PubMed: 21570275]
33. Bache KG, Stuffers S, Malerød L, Slagsvold T, Raiborg C, Lechardeur D, Wälchli S, Lukacs GL, Brech A, Stenmark H. The ESCRT-III subunit hVps24 is required for degradation but not silencing of the epidermal growth factor receptor. Mol Biol Cell. 2006; 17:2513–2523. [PubMed: 16554368]
34. Wollert T, Hurley JH. Molecular mechanism of multivesicular body biogenesis by ESCRT complexes. Nature. 2010; 464:864–869. [PubMed: 20305637]
35. Trajkovic K, Hsu C, Chiantia S, Rajendran L, Wenzel D, Wieland F, Schwille P, Brugger B, Simons M. Ceramide triggers budding of exosome vesicles into multivesicular endosomes. Science. 2008; 319:1244–1247. [PubMed: 18309083]
36. Matsuo H, Chevallier J, Mayran N, Le Blanc I, Ferguson C, Faure J, Blanc NS, Matile S, Dubochet J, Sadoul R, Parton RG, Vilbois F, Gruenberg J. Role of LBPA and Alix in multivesicular liposome formation and endosome organization. Science. 2004; 303:531–534. [PubMed: 14739459]
37. Falguieres T, Luyet PP, Bissig C, Scott CC, Velluz MC, Gruenberg J. In vitro budding of intralumenal vesicles into late endosomes is regulated by Alix and Tsg101. Mol Biol Cell. 2008; 19:4942–4955. [PubMed: 18768755]
38. Schnupf P, Portnoy DA, Decatur AL. Phosphorylation, ubiquitination and degradation of listeriolysin O in mammalian cells: role of the PEST-like sequence. Cell Microbiol. 2006; 8:353–364. [PubMed: 16441444]

39. Tsai YC, Maditz R, Kuo CL, Fishman PS, Shoemaker CB, Oyler GA, Weissman AM. Targeting botulinum neurotoxin persistence by the ubiquitin-proteasome system. Proc Natl Acad Sci U S A. 2010; 107:16554–16559. [PubMed: 20823219]

40. Slot JW, Geuze HJ. A new method of preparing gold probes for multiple-labeling cytochemistry. Eur J Cell Biol. 1985; 38:87–93. [PubMed: 4029177]

41. Tokuyasu KT. A technique for ultracryotomy of cell suspensions and tissues. J Cell Biol. 1973; 57:551–565. [PubMed: 4121290]

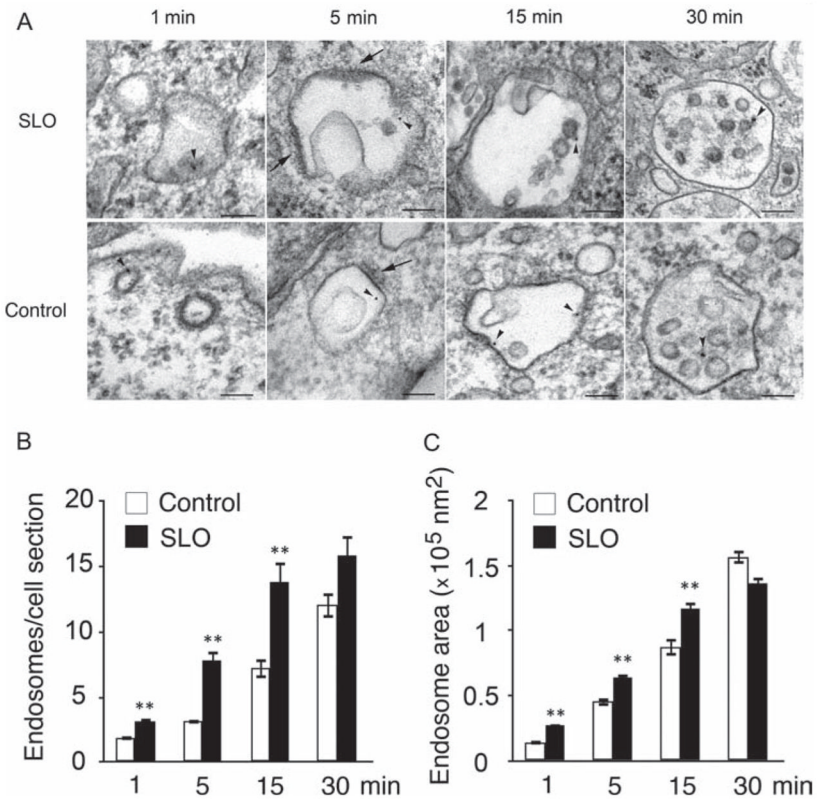

Figure 1. Cell permeabilization with SLO induces formation of endosomes that increase in size over time

Cells were incubated or not with 250 ng/mL SLO for 5 min at 4°C, washed and shifted to 37°C in the presence of Ca^{2+} for increasing periods of time in the presence of BSA-gold as an endocytic tracer. A) Representative TEM images of endosomes containing BSA-gold (arrowheads) at various time-points. BSA-gold-positive endosomes with flat electron-dense coats on their limiting membrane (arrows) increase in size and acquire internal vesicles over time. Bars = 100 nm. B) Quantification of BSA-gold-containing endosomes show a significant increase in newly formed endosomes from 1 to 15 min after permeabilization in SLO-treated cells, when compared to control cells. C) Endosome area is significantly larger in SLO-treated cells from 1 to 15 min after permeabilization, when compared to control cells. Results are expressed as mean ± SEM. **$p < 0.01$, unpaired Student's *t*-test.

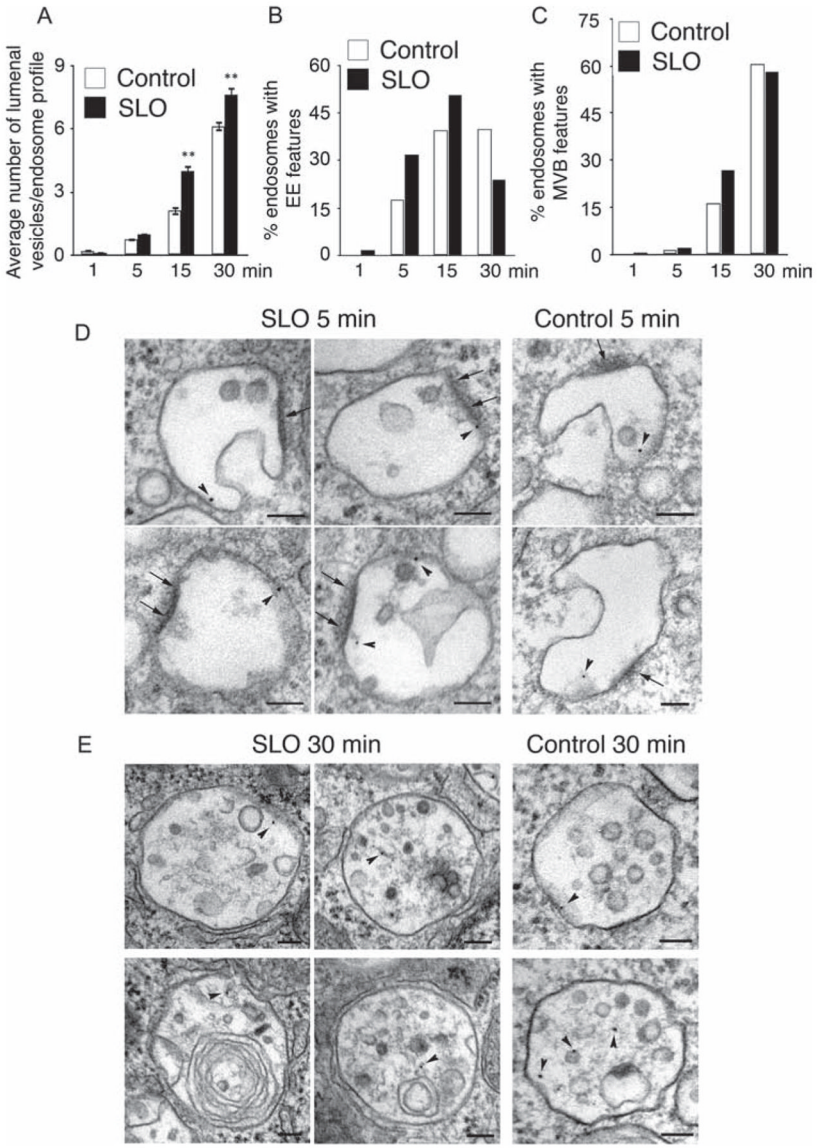

Figure 2. SLO-induced endosomes gradually acquire features of early and late endosomes

Cells were treated as described in Figure 1. A) The average number of internal vesicles per endosome profile increases over time in both control and SLO-permeabilized cells, but is significantly higher after 15 and 30 min of SLO treatment, when compared to control cells. Results are expressed as the mean ± SEM. **$p < 0.01$, unpaired Student's *t*-test. B) The percentage of early endosome-like vesicles (showing flat electron-dense coats and no more than five intraluminal vesicles) is higher between 1 and 15 min after SLO permeabilization, followed by a decrease after 30 min. C) The percentage of MVB-like vesicles (containing six or more intraluminal vesicles) is higher after SLO permeabilization between 1 and 15 min, but is similar to control cells after 30 min. D) Representative TEM images of vesicles containing BSA-gold (arrowheads) and showing morphological features of early endosomes, after 5 min in control and SLO-treated cells. Arrows indicate electron-dense areas on the limiting membrane reminiscent of flat clathrin coats characteristic of early endosomes. E) Representative TEM images of vesicles containing BSA-gold (arrows) showing the characteristic MVB/lysosome morphology, after 30 min in control and SLO-treated cells.

The images show the numerous intraluminal vesicles and occasional multilamellar structures inside endosomes. Bar = 100 nm.

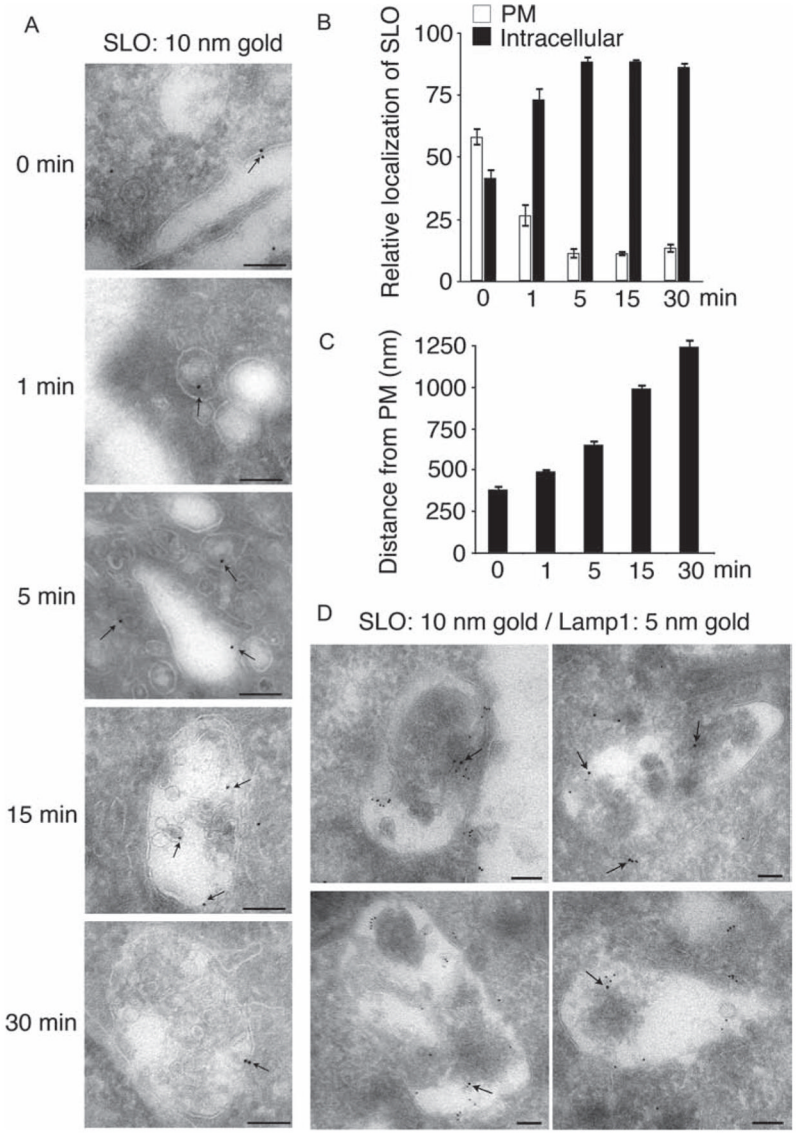

Figure 3. SLO is removed from the plasma membrane of permeabilized cells and traffics to MVB/lysosomes

Cells were treated with 250 ng/mL GFP-SLO at 4°C for 5 min, washed and shifted to 37°C in the presence of Ca^{2+} for increasing periods of time. Samples were then fixed and processed for cryo-immuno EM and stained with anti-GFP and/or anti-Lamp1 antibodies. A) Cryo-immuno EM localization of GFP-SLO (arrows) at the plasma membrane immediately after permeabilization (0 min) and on increasingly larger endocytic vesicles over time (1–30 min). Bar = 100 nm. B) The percentage of the total SLO detected at the plasma membrane decreases from ~ 60% at 0 min to about 12% as early as 5 min after cell permeabilization, while a corresponding increase is seen in intracellular SLO. C) The distance (nm) of intracellular SLO to the plasma membrane increases progressively over time. Quantifications were performed in 10–17 cells containing 175–500 gold particles. Results are expressed as the mean ± SEM. D) Representative cryo-immuno EM images of GFP-SLO (10-nm gold) and Lamp1 (5-nm gold) staining in cells treated with GFP-SLO for 30 min. GFP-SLO and Lamp1 staining colocalize on endosomal structures containing intraluminal vesicles at 30 min after cell permeabilization and repair. Bar = 100 nm.

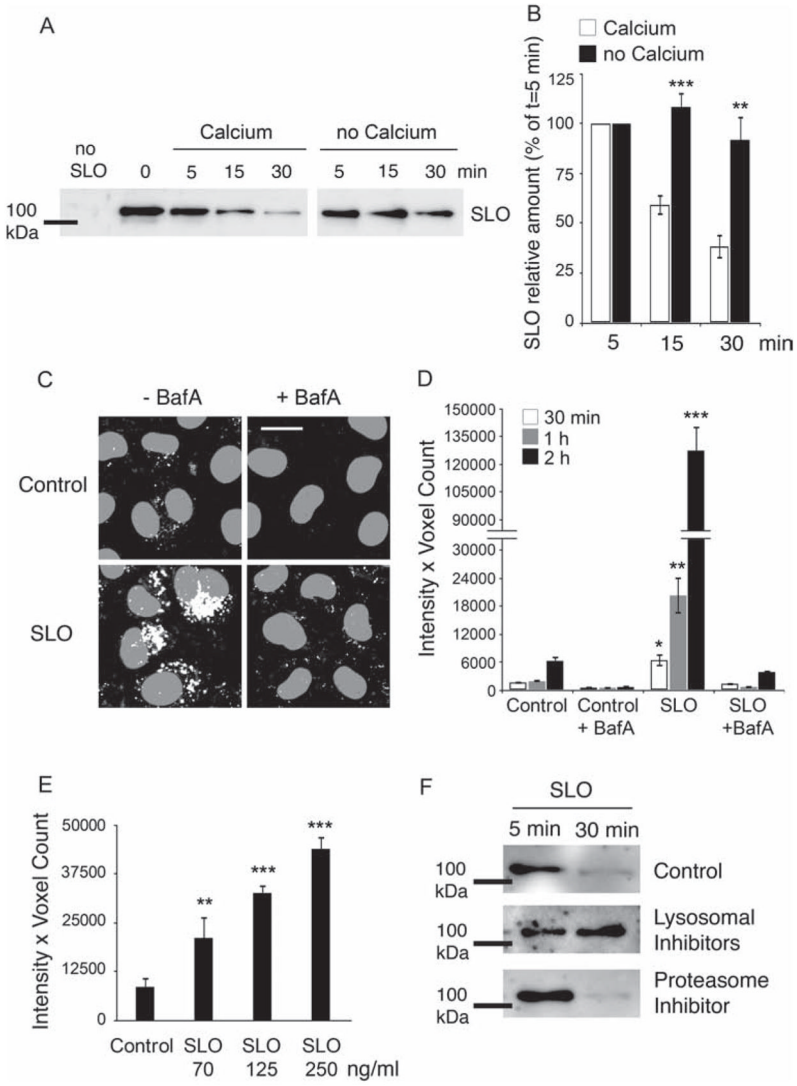

Figure 4. SLO-induced endosomes mature into acidic compartments, where SLO is degraded by lysosomal enzymes

A and B) Cells were incubated with GFP-SLO (250 ng/mL) for 5 min at 4°C, washed and shifted to 37°C in medium containing or not Ca^{2+} for increasing periods of time. Cell extracts are then incubated with GFP-Trap for pulldown of total GFP-SLO and analyzed by western blot. A) GFP-SLO immunoblot at increasing periods after cell permeabilization in the presence (repair conditions) or absence (no repair conditions) of Ca^{2+}. The amount of cell-associated GFP-SLO decreases rapidly between 5 and 30 min in cells permeabilized in the presence but not in the absence of Ca^{2+}. B) Densitometric quantification of GFP-SLO after various time-points in the presence or absence of Ca^{2+}, expressed as percentage of the amount detected at $t = 5$ min. Results are expressed as the mean ± SEM of eight independent experiments. **p < 0.01, ***p < 0.001, unpaired Student's *t*-test. C–E) Cells were incubated with SLO for 5 min at 4°C followed by a 10-min incubation at 37°C with DQ-BSA and chased for increasing periods of time. C) Representative images of cells treated or not with 250 ng/mL SLO and incubated with DQ-BSA, followed by a chase for 2 h in the presence or absence of BafA. SLO treatment leads to a marked enhancement in DQ-BSA fluorescence, reflecting the increased number of acidified late endocytic compartments. Blocking acidification with BafA abolishes DQ-BSA fluorescence. DQ-BSA fluorescence is depicted

in white and DAPI-stained nuclei in gray. Bar = 5 μm. D) Quantification of DQ-BSA fluorescence intensity in control and SLO-treated cells over time. Exposure to SLO progressively increases the fluorescence intensity of DQ-BSA over a 30-, 60- and 120-min chase period, reflecting acidification of the endocytic compartments induced by the toxin. The values reflect the mean fluorescence intensity of five independent microscopic fields per sample. E) SLO permeabilization causes a dose-dependent increase in the fluorescence intensity of endocytosed DQ-BSA after a 2-h chase. Results in (E and F) are expressed as the mean ± SEM. *$p < 0.05$, **$p < 0.01$, ***$p < 0.005$, unpaired Student's *t*-test comparing all samples to the untreated control. F) Control cells or cells treated with concanamycin A/leupeptin or MG132 were incubated with GFP-SLO (250 ng/mL) for 5 min at 4°C, shifted to 37°C in medium containing Ca^{2+} for 5 or 30 min and processed for GFP pulldown and immunoblot. Lysosomal, but not proteasome, inhibitors blocked GFP-SLO degradation.

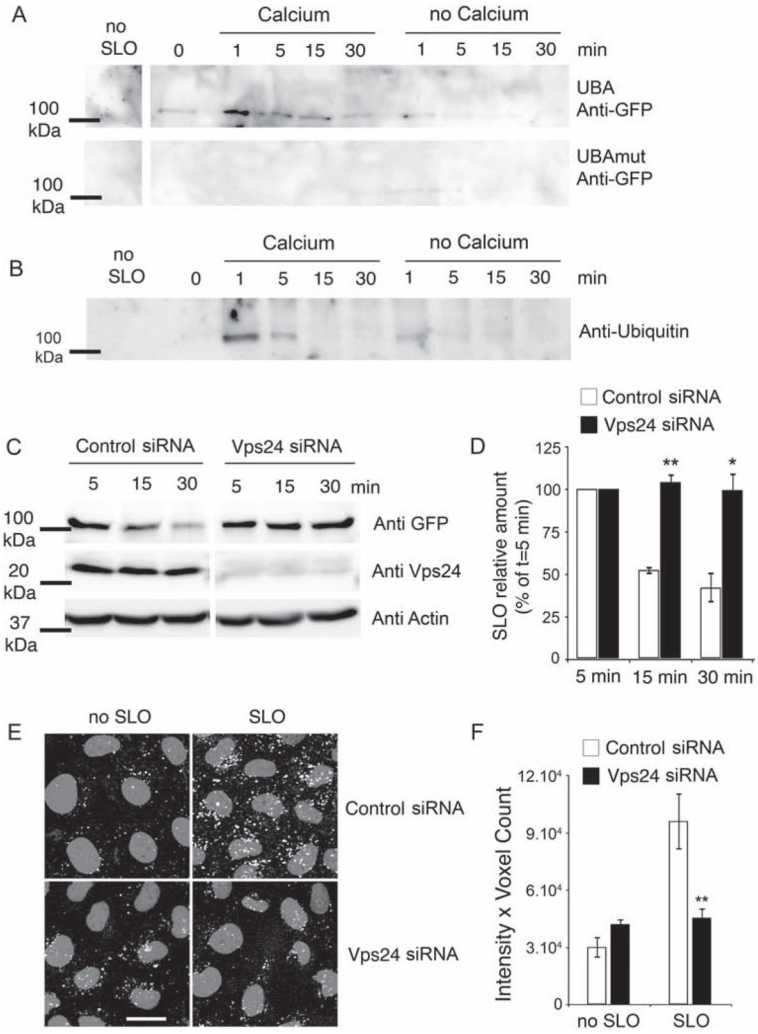

Figure 5. After endocytosis, SLO is ubiquitinated and sorted by the ESCRT complex into the lumen of MVBs for degradation

A and B) Cells were incubated for 5 min at 4°C with 150 and 250 ng/mL GFP-SLO, respectively, washed and shifted to 37°C in medium with or without Ca^{2+} followed by solubilization and pulldown of ubiquitinated proteins using UBA-agarose (A) or pulldown of GFP-SLO using GFP-Trap (B). A) Ubiquitinated GFP-SLO is detected by immunoblot with anti-GFP antibodies after 1 min in the presence of Ca^{2+}, and then decreases over time. Without Ca^{2+} and in control UBAmut pulldowns, only trace amounts of ubiquitinated GFP-SLO are detected. B) Ubiquitinated GFP-SLO is detected by immunoblot using anti-ubiquitin after 1 min in the presence of Ca^{2+} and then decreases over time. Without Ca^{2+}, only a low amount of ubiquitinated SLO is detectable. C and D) Cells treated with control or Vps24 siRNA were exposed to GFP-SLO, followed by pulldown and immunoblot to assess GFP-SLO intracellular degradation. C) Immunoblot of GFP-Trap pulldowns shows GFP-SLO degradation between 5 and 30 min in cells treated with control, but not Vps24 siRNA. Immunoblot of cell extracts shows the depletion in Vps24 achieved with the specific siRNA, and the similar amounts of actin detected after treatment with Vps24 or control siRNA. D) Densitometric quantification of GFP-SLO at 15 and 30 min, expressed as percentage of the amount detected at $t = 5$ min. Results are expressed as the mean ± SEM of three independent experiments. $^{**}p < 0.01$, $^{*}p < 0.05$, unpaired Student's *t* test. E and F) Cells treated with

control or Vps24 siRNA were processed for DQ-BSA uptake as described in Figure 4C. E) Acidic vesicles containing fluorescent DQ-BSA in cells treated with control or Vps24 siRNA, exposed or not to SLO. DQ-BSA fluorescence is depicted in white and DAPI-stained nuclei in gray. Bar = 5 μm. F) Quantification of the experiment in (E) shows the enhancement in DQ-BSA fluorescence intensity induced by SLO, and the significant inhibition after treatment with Vps24 siRNA, compared to control siRNA. **$p < 0.01$, unpaired Student's *t*-test.

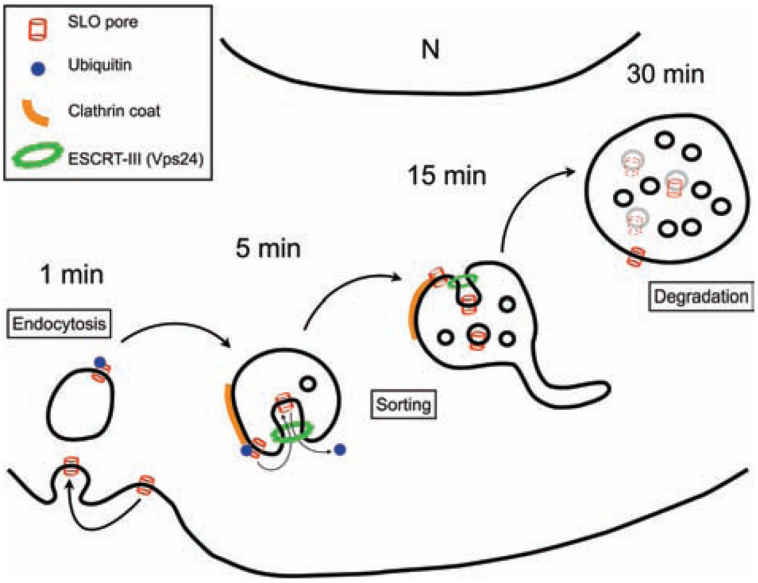

Figure 6. Model for SLO pore endocytosis, trafficking and degradation within the endocytic pathway

When SLO pores form on the plasma membrane, the Ca^{2+}-dependent membrane repair process is induced, promoting endocytosis and rapid ubiquitination of SLO (1 min). Endocytic vesicles carrying ubiquitinated SLO initially show early endosomal features including flat clathrin coats (5 min), and gradually mature into late endosomes/MVBs (15–30 min). This maturation process involves removal of the toxin pores from the limiting membrane, by a luminal budding mechanism dependent on the ESCRT-III complex component Vps24. Sorting of SLO pores into the lumen of MVBs allows vesicle acidification and SLO degradation (30 min).